J Appl Electrochem (2009) 39:2553–2568
DOI 10.1007/s10800-009-9951-x

ORIGINAL PAPER

Electrochemical and molecular dynamics simulation studies on the corrosion inhibition of aluminum in molar hydrochloric acid using some imidazole derivatives

K. F. Khaled · Mohammed A. Amin

Received: 8 February 2009 / Accepted: 8 June 2009 / Published online: 23 June 2009

Abstract The corrosion inhibition and adsorption characteristics of three selected imidazole derivatives namely, 2-amino-4,5-imidazoledicarbonitril (AID), 5-amino-4-imidazolecarboxamide (AIC) and imidazole (IM) on aluminum in 1.0 M HCl was investigated at 25 °C. Measurements were carried out under various experimental conditions using chemical (weight loss), and electrochemical (Tafel polarization and impedance) methods. Molecular dynamics (MD) method and density functional theory were also applied here for theoretical study. Results obtained showed that inhibition efficiency of these compounds increases with increase in their concentrations due to the formation of a surface film on the aluminum surface. Adsorption energy as well as hydrogen bond length calculations showed that AID was the best corrosion inhibitor among the tested imidazole derivatives. Polarization measurements reveal that the selected imidazole derivatives function mainly as cathodic-type inhibitors. Physisorption, followed by chemisorption was proposed as the mechanism for the inhibition process. Adsorption via H-bond formation was also considered here. Results obtained from theoretical study were found to confirm experimental findings.

Keywords Corrosion inhibition · Aluminum · Molecular dynamics simulations · Quantum chemical calculations · Imidazole derivatives

K. F. Khaled (✉)
Electrochemistry Research Laboratory, Chemistry Department, Faculty of Education, Ain Shams University, Roxy, Cairo 11711, Egypt
e-mail: Khaledrice2003@yahoo.com

M. A. Amin
Chemistry Department, Faculty of Science, Ain Shams University, Abbassia, Cairo 11566, Egypt

1 Introduction

Aluminum and its alloys have a low density, an attractive appearance, relatively good corrosion resistance and excellent thermal and electrical conductivity. The combination of these properties makes it a preferred choice for many industrial applications such as automobiles, food handling, containers, electronic devices, building, aviation, etc.[1–3] Various attempts [4–8] have been made to study the corrosion of aluminum and its alloys, and their inhibition by organic inhibitors in acid solutions.

Hydrochloric acid solutions are used for pickling of aluminum and for its chemical or electrochemical etching. It can be important to add a corrosion inhibitor to decrease the rate of aluminum dissolution in such solutions. Thus, numerous studies concerning the inhibition of aluminum corrosion using organic substances have been conducted in acidic and basic solutions [9–12].

The adsorption of these molecules is influenced by their electronic structure, steric factors, aromaticity, electron density at the donor atoms, and *p*-orbital character of donating electrons [13–15]. The adsorption process is also affected by the presence of hetero atoms, such as N, O, P, and S as well as multiple bonds or aromatic rings in their molecular structure which are assumed to be active centers of adsorption [16].

Several attempts have been made to predict corrosion inhibition efficiency with a number of individual parameters obtained via various quantum chemical calculation methods as a tool for studying corrosion inhibitors [17–20]. These trials were aimed to find possible correlations between corrosion inhibition efficiency and a number of quantum molecular properties such as dipole moment (μ), energies of highest occupied (E_{HOMO}) and lowest unoccupied (E_{LUMO}) molecular orbitals and the difference

between them, ΔE, ($\Delta E = E_{HOMO} - E_{LUMO}$), and Mulliken charges as well as some structural parameters.

The present work was designed to study: (i) corrosion inhibition of aluminum in molar hydrochloric acid solutions by 2-amino-4,5-imidazoledicarbonitril (AID), 5-amino-4-imidazolecarboxamide (AIC), and imidazole (IM) using weight loss, Tafel polarization, and impedance techniques; (ii) the relationship between quantum chemical calculations and experimental inhibition efficiencies of the three tested inhibitors by determining various quantum chemical parameters. The reactivity of these compounds was also analyzed through an evaluation of the Fukui indices, using DFT (density function theory) methods.

2 Experimental

2.1 Chemical and electrochemical measurements

Chemical structures of the studied compounds are presented below.

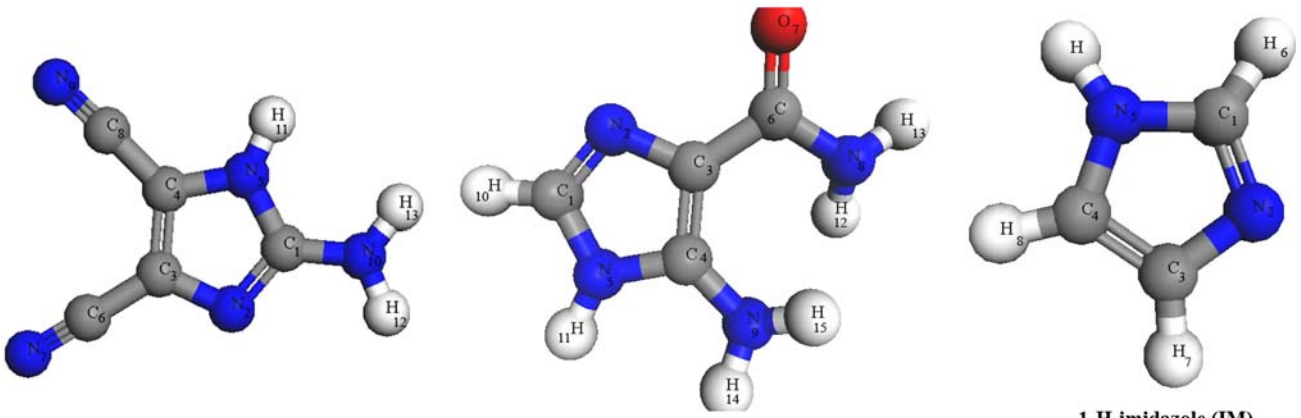

2-Amino-4,5-imidazoledicarbonitril (AID) 5-Amino-4-imidazolecarboxamide (AIC) 1-H-imidazole (IM)

Aluminum specimens from Johnson Mattey (Puratronic, 99.999%) were mounted in Teflon. An epoxy resin was used to fill the space between Teflon and aluminum electrode. The circular cross sectional area of the aluminum rod exposed to the corrosive medium, used in electrochemical measurements, was 0.28 cm^2. Weight loss measurements were carried out using the same aluminum rods, each of 2.50 cm length and 0.5 cm diameter (surface area = 3.925 cm^2). The electrochemical measurements were performed in a typical three-compartment glass cell consisted of the aluminum specimen as working electrode (WE), platinum counter electrode (CE), and a saturated calomel electrode (SCE) as the reference electrode. The counter electrode was separated from the working electrode compartment by fritted glass. The reference electrode was connected to a Luggin capillary to minimize IR drop. Solutions were prepared from bidistilled water of resistivity 13 MΩ cm, the aluminum electrode was polished with different grit emery papers up to 4/0 grade, cleaned with acetone, washed with bidistilled water, and finally dried.

The electrode potential was allowed to stabilize 60 min before starting the measurements. All experiments were conducted at 25 ± 1 °C. The electrolyte solution was made from HCl (Fisher Scientific) and bidistilled water. The inhibitors (Aldrich chemical co.) used without any pretreatments. Measurements were performed using Gamry Instrument Potentiostat/Galvanostat/ZRA. This includes a Gamry Framework system based on the ESA400, Gamry applications that include dc105 for dc corrosion measurements, EIS300 for electrochemical impedance spectroscopy measurements along with a computer for collecting data. Echem Analyst 4.0 Software was used for plotting, graphing, and fitting data.

Tafel polarization curves were obtained by changing the electrode potential automatically from −250 to +250 mV_{SCE} at open circuit potential with scan rate of 1.0 mV s^{-1}. Impedance measurements were carried out in frequency range from 10 kHz to 1.0 mHz with an amplitude of 10 mV peak-to-peak using ac signals at open circuit potential.

2.2 Computational details

The modeling studies were designed to examine imidazole derivatives–surface interactions that lead to optimal molecular binding to the aluminum surface. The studies would seek to compare the energy-minimized binding configurations as well as adsorption energies for the studied imidazoles. The aluminum surface binding energies of these configurations were computed using DMol[3], a high quality quantum mechanics computer program (available

from Accelrys, San Diego, CA). These calculations employed an ab initio, local density functional (LDF) method with a double numeric polarization (DNP) basis set, and a Becke–Perdew (BP) functional.

Molecular simulation studies were performed using Materials studio 4.3 software from Accelrys Inc. [21] which has been used to build the imidazole molecules, aluminum oxide (111) surface, and solvent molecules using the sketching tools in Materials Visualizer. Molecular mechanics tools are used to investigate the Al_2O_3/solvent/imidazole derivatives systems. The key approximation is that the potential energy surface, on which the atomic nuclei move, is represented by a classical forcefield. COMPASS (Condensed-phase Optimized Molecular Potentials for Atomistic Simulation Studies) [22], which used to optimize the structures of all components of the system of interest (Al_2O_3/solvent/imidazole derivatives) and represents a technology break-through in forcefield method. COMPASS is the first ab initio forcefield that enables accurate and simultaneous prediction of chemical properties (structural, conformational, vibrational, etc.) and condensed-phase properties (equation of state, cohesive energies, etc.) for a broad range of chemical systems. It is also the first high quality forcefield to consolidate parameters of organic and inorganic materials.

The first step in this computational study is the preparation of a model of molecules which adsorb on the surface with optimized geometry (i.e., energy minimized). Among the different steps involved in the modeling approach are the construction of the Al_2O_3 surface from its pure crystal, the addition of the imidazole derivatives near to the surface and the definition of the potentials (i.e., the forcefield) to study the liquid–solid interaction. Following these steps, the geometry optimization is performed. In this particular case, the use of molecular mechanics can be seen as a precursor to computationally more expensive quantum mechanical methods. Once the model has been optimized with suitable forcefield (COMPASS), we will be able to simulate a substrate (Al_2O_3 surface) loaded with an adsorbate (i.e., the three selected imidazoles, namely AID, AIC, and IM) taking into consideration the solvent effect. The objective of this computational study is to find low energy adsorption sites to investigate the preferential adsorption for AID, AIC, and IM on Al_2O_3 surface aiming to find a relation between the effect of their molecular structure and their inhibition efficiency.

In order to build Al_2O_3 surface, amorphous cell module has been used to create solvent/imidazoles cell on Al_2O_3 surface. The behavior of AID, AIC, and IM on the surface was studied using molecular dynamics simulations and the COMPASS forcefield. The simulation box ($29.97 \times 29.97 \times 29.96$ Å) with periodic boundary conditions was built to simulate a representative part of an interface devoid of any arbitrary boundary effects. A cutoff distance of 1.0 nm with a spline switching function was applied for the non-bond interactions, i.e., for Coulombic, van der Waals, and hydrogen bond interactions. The cutoff used to select the spline width which specifies the size of the region within which non-bond interactions are splined from their full value to zero. For the actual computation of this interaction energy charge groups are used. The Al_2O_3 crystal is cleaved along with the (1 1 1) plane, thus representing the Al_2O_3 surface. A low energy adsorption site is identified by carrying out a Monte Carlo search of the configurational space of the substrate–adsorbate system as the temperature is slowly decreased.

All structures used in this study are minimized to ensure that the energy results used in calculating the adsorption energy are accurate. It is critically important that when we optimize the structures, we use the same energy minimization settings as we intend to use for calculating the adsorption energy of imidazole derivatives molecules. This includes not only the forcefield, atomic charges, and non-bond summation methods, but also the quality of the energy and geometry optimization calculations and the convergence tolerances used for the minimization.

3 Results and discussions

3.1 Weight loss measurements

Figure 1a shows plots of weight loss versus time in 1.0 M HCl without and with 10^{-4} M AID, AIC or IM at 25 ± 1 °C. The results show that the corrosion rates in both inhibited and uninhibited solutions increased with time. The non-uniformity and non-linearity of the plots suggest that the aluminum corrosion by HCl is a heterogeneous process involving several steps. Similar observations have been reported for aluminum corrosion in other media [23]. Figure 1a also shows that the corrosion rate in uninhibited systems was observed to increase, as expected, with increase in HCl concentration, indicating that the HCl corrosion of aluminum is concentration dependent. Corrosion of aluminum in aqueous solution, which depends on the concentration of anions in solution, has been reported [24, 25]. A general mechanism for the dissolution of aluminum would be similar to that reported by Ford et al. [26] as well as by Nguyen and Foley [24, 27].

$$Al_{(s)} + H_2O \underset{K_2}{\overset{K_1}{\leftrightarrows}} AlOH_{ads} + H^+ + e \quad (1)$$

$$AlOH_{ads} + 5H_2O + H^+ \underset{k_{-2}}{\overset{k_2}{\leftrightarrows}} Al^{3+} \cdot 6H_2O + 2e \quad (2)$$

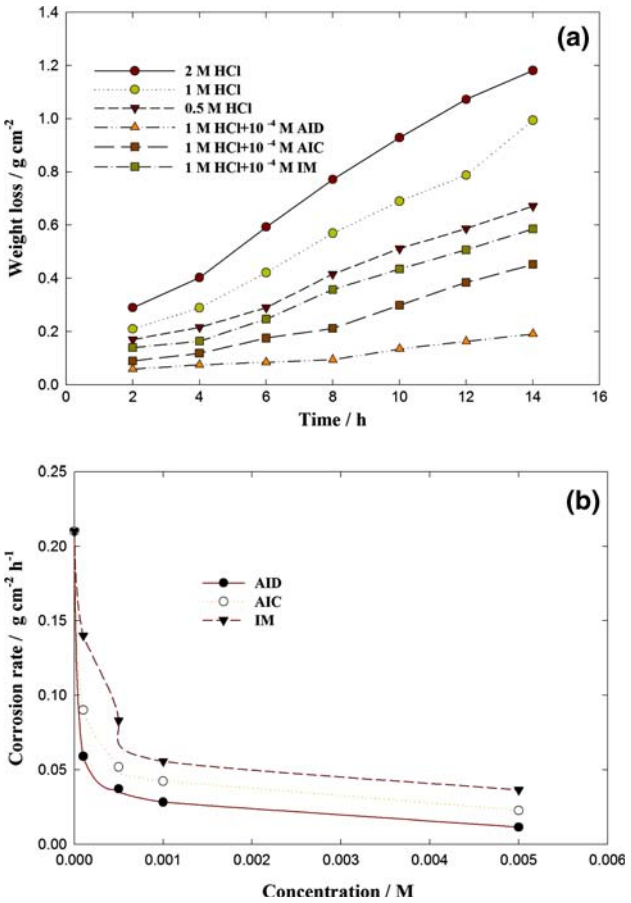

Fig. 1 (**a**) Weight loss versus time curves recorded for Al in HCl solutions of different concentrations and in 1.0 M HCl solutions containing 10^{-4} M AID, AIC or IM 25 ± 1 °C, (**b**) Dependence of corrosion rates (in g cm^{-2} h^{-1}) of the three imidazoles on their concentrations at 25 ± 1 °C

$$Al^{3+} + H_2O \underset{k_{-3}}{\overset{k_3}{\leftrightarrows}} [AlOH]^{2+} + H^+ \quad (3)$$

$$[AlOH]^{2+} + X^- \underset{k_{-4}}{\overset{k_4}{\leftrightarrows}} [AlOHX]^+ \quad (4)$$

The controlling step in the metal dissolution is the complexation reaction between the hydrated cation and the anion, see Eq. 4. In the presence of chloride ions the reaction corresponds to

$$[AlOH]^{2+} + Cl^- \underset{k_{-4}}{\overset{k_4}{\leftrightarrows}} [AlOHCl]^+ \quad (5)$$

The soluble complex ion formed increases the metal dissolution rate which depends on the chloride concentration [24].

Figure 1b shows plots of corrosion rate (expressed in g cm^{-2} h^{-1}) versus imidazole derivatives concentration at 25 ± 1 °C. The various parameters, derived from weight loss measurements, regarding the corrosion of aluminum in 1.0 M HCl solutions without and with various concentrations of the three inhibitors are summarized in Table 1. The inhibition efficiencies of the three tested imidazoles were calculated by using Eq. 6 [28]

Table 1 Corrosion rate in (g cm^{-2} h^{-1}), inhibition efficiency data and surface coverage (θ) obtained from weight loss measurements for Al in 1.0 M HCl solutions without and with various concentrations of AID, AIC or IM at 25 ± 1 °C

Inhibitor	Concentration/ M	Corrosion rate/ g $cm^{-2}h^{-1}$	E_w (%)	θ
	Blank	0.1010	–	–
AID	10^{-4}	0.0295	71.9	0.72
	5×10^{-4}	0.0186	82.3	0.83
	10^{-3}	0.0142	86.5	0.86
	5×10^{-3}	0.0058	94.5	0.94
AIC	10^{-4}	0.0451	57.1	0.57
	5×10^{-4}	0.0260	75.3	0.75
	10^{-3}	0.0212	79.8	0.79
	5×10^{-3}	0.0114	89.2	0.89
IM	10^{-4}	0.0700	33.33	0.33
	5×10^{-4}	0.0415	60.5	0.60
	10^{-3}	0.0279	73.5	0.73
	5×10^{-3}	0.0182	82.6	0.82

$$IE_w\% = \left(1 - \frac{CR_{corr}}{CR^0_{corr}}\right) \times 100 \quad (6)$$

where CR^o_{corr} and CR_{corr} are corrosion rates without and with different concentrations of imidazole derivatives, respectively. It is obvious from Fig. 1b and the data presented in Table 1, that the corrosion rate decreases, corresponding to increased inhibition efficiency the concentrations of the imidazole derivatives increase. This decrease in corrosion rate, and the corresponding increase in efficiency, enhances in the order: IM < AIC < AID. These findings reflect, as will be seen and fully discussed, the highest inhibition performance of AID as compared with IM and AIC. These selected imidazoles, therefore inhibit aluminum corrosion in HCl to an extent depending on inhibitor concentration and its type.

3.2 Tafel polarization measurements

Corrosion parameters were calculated on the basis of Tafel polarization potential–current characteristics in the vicinity of the corrosion potential ($E = E_{corr} \pm 15$ mV) according to the following equations:

$$\log i_a = \log i_{corr} + \frac{E_i - E_{corr}}{b_a} \quad (7)$$

$$\log i_c = \log i_{corr} + \frac{E_i - E_{corr}}{b_c} \quad (8)$$

These equations corresponded to linear anodic and cathodic Tafel lines. Corrosion current density i_{corr} was determined by extrapolating the Tafel lines to $E = E_{corr}$ or according to the Stern–Geary equation.

$$i_{corr} = \frac{b_a b_c}{2.303(b_a + b_c)R_p} \quad (9)$$

where b_a and b_c are the Tafel slopes, R_p is the polarization resistance, defined as the tangent of a polarization curve at E_{corr}.

$$R_p = \left(\frac{dE}{di}\right)_{E=E_{corr}} \quad (10)$$

The anodic and cathodic polarization curves of aluminum in HCl solutions devoid of and containing different concentrations of the three imidazole derivatives are presented in Fig. 2.

Table 2 presents the electrochemical parameters (E_{corr}, i_{corr}, b_a, b_c, and R_p) associated with polarization measurements at various concentrations of imidazole derivatives. Inhibition efficiency $(IE_p\%)$ values were calculated, based on Eq. 11, and also included in Table 2:

$$IE_p\% = \left(1 - \frac{i_{corr}}{i^o_{corr}}\right) \times 100 \quad (11)$$

where i^o_{corr} and i_{corr} are corrosion current density values without and with imidazole derivatives, respectively. Accurate evaluation of corrosion rate (i.e., corrosion current density, i_{corr}) from the anodic branches, and therefore the anodic Tafel slope (b_a), is impossible, simply because the experimental anodic polarization curves presented in Fig. 2 deviate from the Tafel behavior. Since the absence of linearity in the anodic branches prevents linear extrapolation to the corrosion potential, E_{corr}. Consequently, the values of b_a, calculated using the Gamry software, are not included here.

It has been shown that in the Tafel extrapolation method, use of both the anodic and cathodic Tafel regions is undoubtedly preferred over the use of only one Tafel region [29]. However, the corrosion rate can also be determined by Tafel extrapolation of either the cathodic or anodic polarization curve alone. If only one polarization curve alone is used, it is generally the cathodic curve which usually produces a longer and better defined Tafel region. Anodic polarization may sometimes produce concentration effects, due to passivation and dissolution, as noted above, as well as roughening of the surface which can lead to deviations from Tafel behavior.

The cathodic part of the polarization curves in Fig. 2 is under activation control and exhibits linearity in accord with Tafel relationship. The corrosion rate, and therefore the cathodic Tafel slope, b_c, may be estimated accurately by extrapolating the cathodic linear region back to E_{corr}. Analysis of the polarization curves in Fig. 2 as well as the data in Table 2 shows that the increase in concentration of each inhibitor leads to a displacement of the polarization

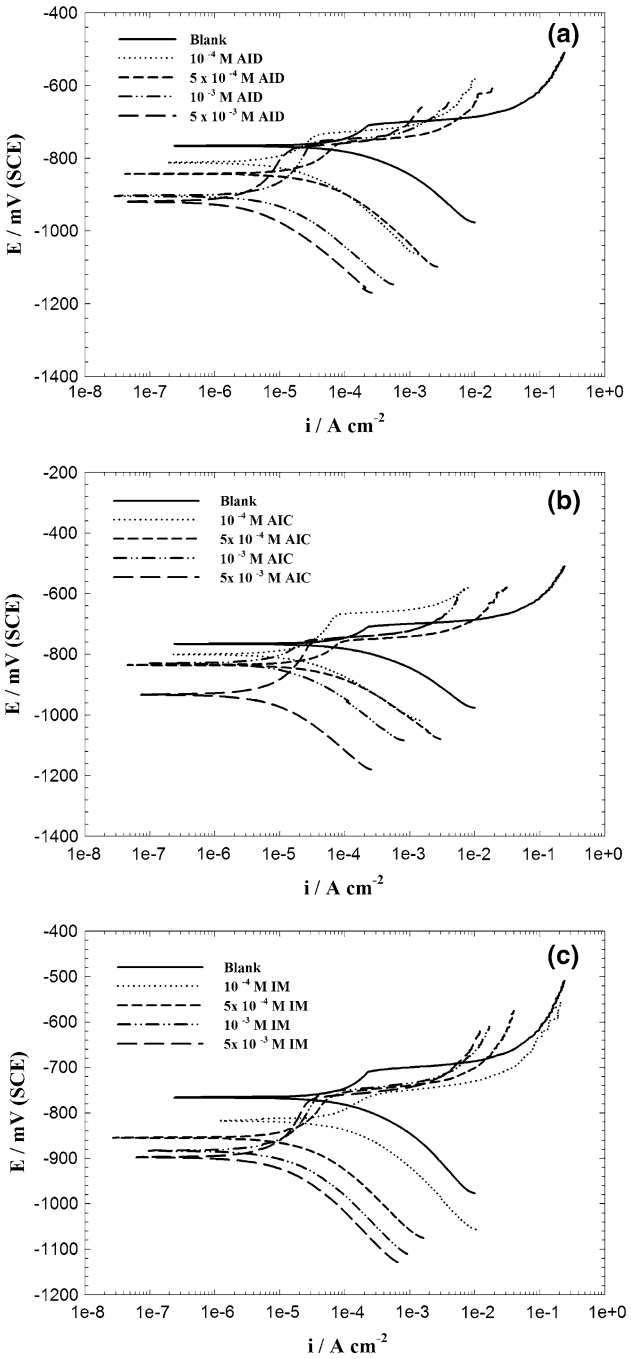

Fig. 2 Anodic and cathodic polarization curves recorded for Al in 1.0 M HCl solutions without and with various concentrations of **a** AID; **b** AIC; **c** IM, at 25 ± 1 °C

Table 2 Electrochemical kinetic parameters obtained by Tafel polarization technique for Al in 1.0 M HCl solutions without and with various concentrations of AID, AIC or IM at 25 ± 1 °C

Inhibitor	Concentration/M	i_{corr}/μA cm^{-2}	$-E_{corr}$/mV (SCE)	$-\beta_c$/mV dec^{-1}	C.R mpy	R_p/kΩ cm^2	E_p (%)
	Blank	64.96	766.2	91.66	27.86	0.622	–
AID	10^{-4}	22.21	811.5	110.9	9.525	5.844	65.81
	5×10^{-4}	14.16	842.9	105.8	6.073	2.846	78.20
	10^{-3}	12.06	903.2	120.3	5.174	11.98	81.43
	5×10^{-3}	5.195	919.4	121.9	2.228	28.15	92.01
AIC	10^{-4}	31.86	800.4	135.4	13.67	4.22	50.95
	5×10^{-4}	18.70	836.0	104.1	8.021	2.358	71.21
	10^{-3}	16.17	830.0	153.6	6.935	8.707	75.11
	5×10^{-3}	10.96	933.4	186.7	4.701	16.30	83.13
IM	10^{-4}	45.65	816.8	97.4	19.58	0.805	29.72
	5×10^{-4}	29.99	854.6	130.9	12.86	4.15	53.83
	10^{-3}	20.75	883.1	140.3	9.901	7.576	68.06
	5×10^{-3}	14.82	897.7	142.6	6.82	10.78	77.18

curves toward more negative potential values, and a noticeable decrease in i_{corr} results [30].

The addition of the three inhibitors individually enhances both anodic and cathodic overpotentials. However, the cathodic overvoltage is much greater than the anodic one. In this case, the rate of cathodic reaction controls the rate of corrosion. This means that the cathodic process is highly suppressed by the inhibitor addition. Thus, each compound of the three tested imidazoles acts mainly as a cathodic-type inhibitor to the corrosion of Al, by retarding hydrogen evolution on cathodic sites of the electrode surface. The cathodic inhibitive action of these compounds may be interpreted on the basis that the potential at the cathodic sites is more positive than that at the anodic sites, and therefore the inhibitor adsorption, as will be discussed latter, is more likely at the cathodic sites, resulting in a marked increase in the cathodic overpotential.

It follows from Fig. 2 that the shapes of the polarization plots for inhibited electrodes are not substantially different from those of uninhibited electrodes. The presence of each inhibitor decreases the corrosion rate but does not change other aspects of the behavior. This means that the inhibitor does not alter the electrochemical reactions responsible for corrosion. In all cases it is observed that the hydrogen evolution reaction is activation controlled since the cathodic portions rise to Tafel lines. It is clear that the mechanism of proton reduction is not modified upon surfactant addition. This is clearly seen from the low variation in the cathodic Tafel slope (b_c), inspect Table 2. The absence of significant changes in the cathodic Tafel slope in the presence of each inhibitor indicates that the hydrogen evolution is slowed by the surface blocking effect of the inhibitor. The inhibitive action of these three imidazoles, therefore may be related to their adsorption and formation of a barrier film on the electrode surface, protecting it from corrosion.

3.3 Impedance measurements

The effects of the imidazole derivatives with various concentrations on the impedance behavior of pure aluminum in 1.0 M HCl solution have been studied at the respective corrosion potentials at 25 °C. Nyquist plots and the corresponding Bode plots are depicted in Fig. 3. The shape of the impedance diagrams of aluminum in acidic solution is similar to those found in the literature [31, 32]. The presence of imidazole derivatives increases the impedance but does not change the other aspects of corrosion mechanism occurred due to their addition. The Nyquist plots presented in Fig. 3a are characterized by three time constants, namely: (1) a capacitive time constant at high frequency values, (2) an inductive time constant at medium frequencies, and (3) a second capacitive time constant at low frequencies. In the literature there is no consensus about the origin of the time constants of the impedance diagram. The time constant at high frequencies is attributed to the formation of the oxide layer or to the oxide layer itself. Brett [33] assigns the high frequency time constant to the reactions involved at the formation of the oxide layer. He suggested that at the metal-oxide interface aluminum is oxidized to Al^+intermediates. The Al^+ intermediates will subsequently be oxidized to Al^{3+} at the oxide–solution interface where also O^{2-} or OH^- is formed. Simultaneously with the formation of O^{2-} ions, H^+ ions are formed. This results in a local acidification at the oxide-electrolyte interface. The other possible explanation for the

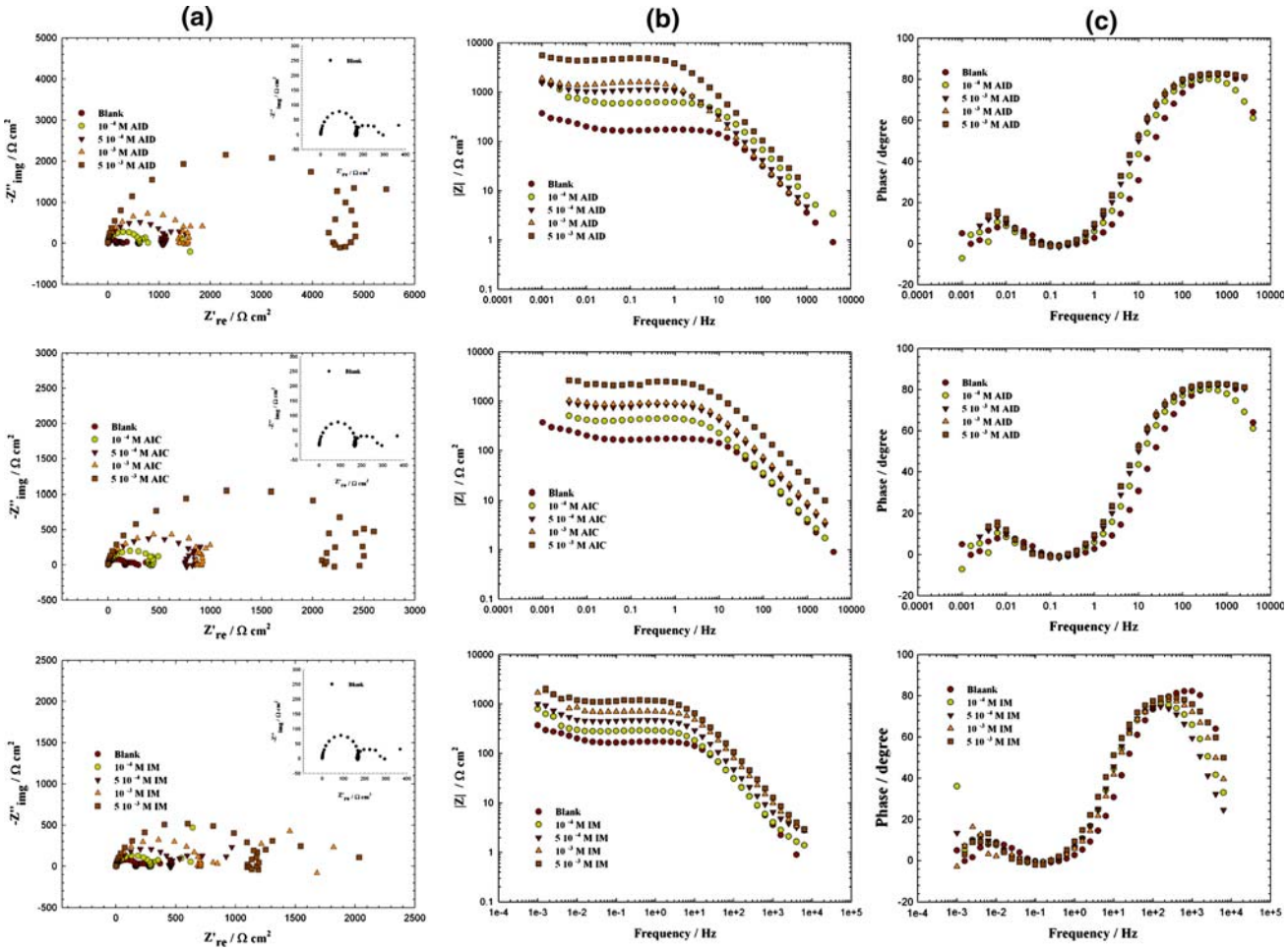

Fig. 3 Nyquist and Bode plots recorded for Al in 1.0 M HCl solutions without and with various concentrations of **a** AID; **b** AIC; **c** IM, at the respective corrosion potentials at 25 ± 1 °C

capacitive time constant at high frequencies is the oxide film itself which is considered as a parallel circuit of a resistor due to ionic conduction in the oxide, and a capacitance due to the dielectric properties of the oxide. The inductive time constant at medium frequencies often attributed to surface or bulk relaxation of species in the oxide [34]. Adsorption of intermediates (H^+ and Cl^-ions) could also cause an inductive loop.

Equivalent circuit inserted in Fig. 4 was used to model the impedance data, as previously reported [35]. The model includes the solution resistance, R_s, a series combination of resistance, R, and inductance, L, in parallel with charge transfer resistance $(R_{ct})_1$, and the constant phase element (CPE_1). In the high frequency limit, the inductive contribution to the overall impedance is insignificant. Therefore, Nyquist plot of the impedance is a semicircle characteristic of the parallel arrangement of the double layer capacitance and charge transfer resistance corresponding to the aluminum dissolution reaction. Contribution to the total impedance at intermediate frequencies comes mainly from the charge transfer resistance and inductive component in parallel. The inductor arises from adsorption effects of the oxide film and/or imidazole derivatives and could be define as $(L = R\tau)$ where τ is the relaxation time for adsorption on aluminum surface. The low frequency locus displays the characteristics of parallel RC circuit. This circuit includes another constant phase element (CPE_2) which is placed in parallel to charge transfer resistance element $(R_{ct})_2$. The $(R_{ct})_2$ value is a measure of charge transfer resistance corresponds to the $Al^+ \rightarrow Al^{3+}$ reaction.

The CPE is used in this model to compensate for non-homogeneity in the system and is defined by two values, Q and n. The impedance of CPE is represent by

$$Z_{CPE} = Q^{-1}(i\omega)^{-n} \tag{12}$$

where $i = (-1)^{1/2}$, ω is the frequency in rad s^{-1}, $\omega = 2\pi f$ and f is the frequency in Hz. If $n = 1$, the impedance of CPE is identical to that of a capacitor, $Z_C = (i\omega C)^{-n}$, and

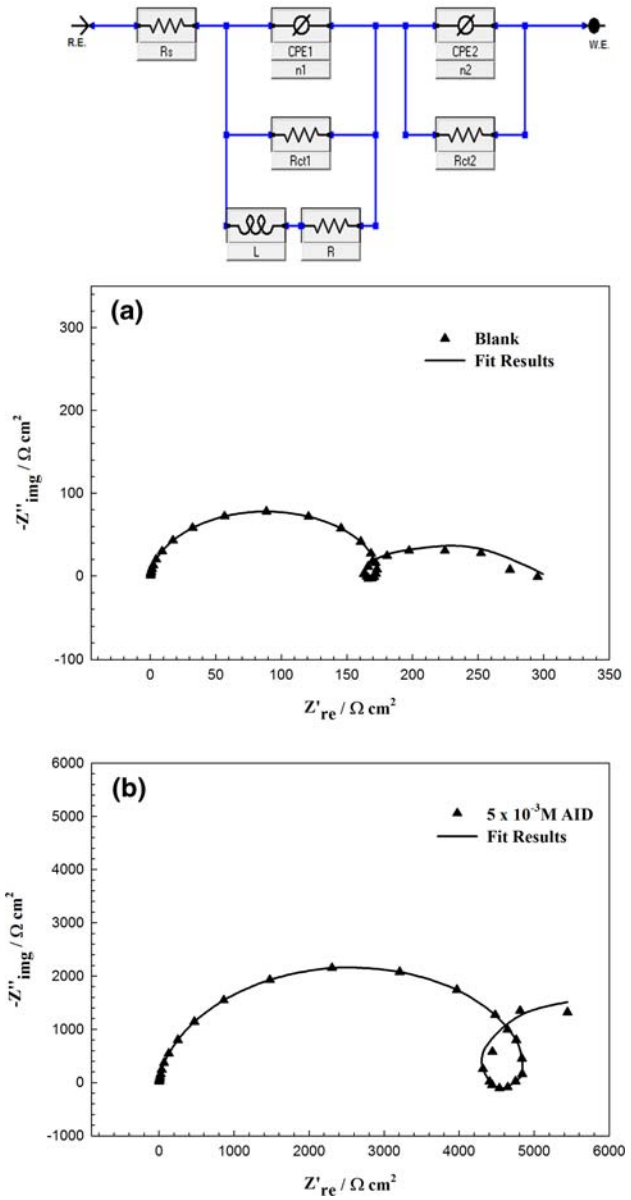

Fig. 4 Experimental and computer fit results of Nquist plot recorded for Al in 1.0 M HCl without (**a**) and with 5.0×10^{-3} M AID (**b**). Inset of **a**: the equivalent circuit used to fit the experimental impedance data

in this case Q gives a pure capacitance (C). For non-homogeneous system, $n < 1$.

Computer fitting of the spectrum allows evolution of the elements of the circuit analog. The aim of the fitting procedure is to find those values of the parameters which best describe the data, i.e., the fitting model must be consistent with the experimental data. Representative examples for the experimental and computer fit results of Nyquist plot for Al in 1.0 M HCl in the absence and presence of imidazole derivatives are demonstrated in Fig. 4. The points in Fig. 4 represent the experimental data, while the solid lines represent the best fits. The numerical values of the fitting parameters including polarization resistance $R_p = (R_{ct})_1 + (R_{ct})_2$ are presented in Table 3 and were determined by analysis of the complex plane impedance plots and the equivalent circuit model by means of a computer program (Echem Analyst 5.5 from Gamry).

The experimental data were found to be sufficiently well fitted by the transfer function of the equivalent circuit inserted in Fig. 4 within the limits of experimental error and reproducibility of the data. Table 3 shows the impedance parameters recorded for aluminum in 1.0 M HCl solution in absence and presence of various concentrations of the three imidazole derivatives at 25 ± 1 °C. The values of the polarization resistance, R_p, increase with increase in concentrations of inhibitors showing that the inhibition efficiency of these molecules increases as their concentration increases. The inhibition efficiency obtained from impedance measurements are calculated using Eq. 13.

$$IE_i\% = \left(1 - \frac{R_p^o}{R_p}\right) \times 100 \tag{13}$$

where $R_p^o$and R_p are the polarization resistances for uninhibited and inhibited solutions, respectively. Inspection of Table 3 shows that R_p and double layer capacitance C_{dl} modeled as Q_1, have opposite trend at the whole concentration range. It can be supposed that a protective layer covers the surface of the electrode. Its nature can be some solid film, inhibiting species or both. The decrease in this capacitance Q_1 with increase in imidazole derivatives concentrations may be attributed to the formation of a protective layer on the electrode surface [36]. The thickness of this protective layer increases with increase in inhibitor concentration, since more inhibitor molecules electrostatically adsorb on the electrode surface, resulting in a noticeable decrease in Q_1. This trend is in accordance with Helmholtz model, given by Eq. 14 [37]:

$$C_{dl} = \frac{\varepsilon \varepsilon_o A}{d} \tag{14}$$

where d is the thickness of the protective layer, ε is the dielectric constant of the medium, ε_0 is the vacuum permittivity, and A is the effective surface area of the electrode.

Bode plots shown in Fig. 3b, exhibit three distinctive segments. In the higher frequency region with increasing frequency the log |Z| values tend to become zero and the phase angle values falling rapidly toward 0°. This is a response of resistive behavior and corresponds to the solution resistance. In the medium frequency region, a linear relationship between log |Z| against log f, with a slop near to −1 and the phase angle tends to become −90°, can be observed. This response is a characteristic of capacitive behavior. An ideal capacitive response would result in a

Table 3 The computer fit results for the experimental impedance data recorded for Al in 1.0 M HCl solutions without and with various concentrations of AID, AIC or IM at the respective corrosion potentials at 25 ± 1 °C

Inhibitor		R_s/Ω cm^2	Q_1/μFcm^{-2}	n_1	$(R_{ct})_1/\Omega$cm^2	L/Hcm^2	R/Ω cm^2	Q_2/mFcm^{-2}	n_2	$(R_{ct})_2/\Omega$cm^2	R_p/Ωcm^2	E_i (%)
	Blank	1.2	20	0.91	170	8	300	15.2	0.89	134		–
AID	10^{-4}	2.3	13.5	0.89	510.5	35	1,178	35.1	0.89	590.5	1101.05	72.39
	5×10^{-4}	3.4	9.6	0.85	894.1	44	15,648	41.2	0.91	1033.6	1927.71	84.23
	10^{-3}	3.1	8.5	0.83	1200.0	59	1,897	49.5	0.90	1387.2	2587.23	88.25
	5×10^{-3}	3.2	3.2	0.83	3810.8	72	5,897	55.6	0.91	4405.4	8216.21	96.30
AIC	10^{-4}	2.5	14.1	0.83	344.5	28	980	28.6	0.93	398.53	743.094	59.09
	5×10^{-4}	3.1	12.3	0.87	649.1	33	1,325	36.5	0.91	751.15	1400.27	78.29
	10^{-3}	5.1	10.7	0.86	750.0	39	1,645	44.2	0.92	867.02	1617.02	81.20
	5×10^{-3}	3.2	9.5	0.84	1826.1	46	1,894	48.6	0.90	2116.8	3942.93	92.29
IM	10^{-4}	3.2	18.2	0.82	240.1	22	875	22.6	0.91	277.68	517.799	41.29
	5×10^{-4}	3.4	15.3	0.81	386.1	30	1,154	26.7	0.92	446.57	832.648	63.49
	10^{-3}	2.9	12.2	0.91	589.9	33	2,045	30.1	0.92	682.01	1271.96	76.10
	5×10^{-3}	2.5	10.9	0.92	951.3	38	3,210	36.1	0.96	1101.3	2052.66	85.19

slope of −1 and a phase angle of −90°; however, it is well known that an electrochemical system generally does not behave in an ideal manner. In the low frequency region, the resistive behavior of the electrode increases, but the region where log |*Z*| does not depend on log *f*, i.e., dc limit is not completely reached [38, 39]. Figure 3c presents the impedance diagrams for the same experimental data in Bode-phase format for aluminum in 1.0 M HCl in the absence and presence of imidazole derivatives. Two time constants can be observed which indicated that imidazole derivatives acted through forming a film for protection against corrosion. Furthermore, the maximum phase angle increases as inhibitor concentration increases, indicating that the double layer capacitance values are decreasing, as in Table 3. This behavior confirms the adsorption action of imidazole derivatives against aluminum corrosion [39].

It is worth noting from Tables 1, 2, and 3 that the inhibition efficiency values obtained from weight loss and impedance measurements are comparable and run parallel with those obtained from polarization measurements. The little difference found in results obtained from both electrochemical and weight loss measurements was also reported by several authors [40]. This little difference in inhibition efficiency values between weight loss and electrochemical measurements suggests that a long-term prediction of uniform corrosion can be achieved in this case by the less-time consuming electrochemical techniques of a dc Tafel polarization and ac impedance.

3.4 Computational results

Molecular modeling studies give indications of a strong molecular attraction to the metal to better understand the performance mechanism for the imidazole derivatives. The modeling studies were designed to examine this theory by predicting the inhibitor-surface interactions that lead to optimal molecular binding at the aluminum surface.

In Monte Carlo simulation, molecular dynamics were performed on a system comprising imidazole derivatives, solvent molecules, and Al_2O_3 surface. Each imidazole derivative is placed on the Al_2O_3 surface, optimize and then run quench molecular dynamics. Total energy, average total energy, Van der Waals energy, electrostatic energy, and intramolecular energy for the studied system are presented in Fig. 5 (representative example for optimization energy of of Al_2O_3/solvent/inhibitor system). Monte Carlo docking was done on each of the 100 conformations, and each of the docked structures was energetically relaxed.

The Monte Carlo simulation process tries to find the lowest energy for the whole system. The structures of the adsorbate components are minimized until they satisfy certain specified criteria. The outputs and descriptors calculated by the Monte Carlo simulation are presented in Table 4. The parameters presented in Table 4 include total energy of the substrate–adsorbate configuration. The total energy is defined as the sum of the energies of the adsorbate components, the rigid adsorption energy, and the deformation energy. In this study, the substrate energy (Al_2O_3 surface) is taken as zero. Also, adsorption energy reports energy released (or required) when the relaxed adsorbate components are adsorbed on the substrate.

The adsorption energy is defined as the sum of the rigid adsorption energy and the deformation energy for the adsorbate components. The rigid adsorption energy, reports the energy, in kcal mol^{-1}, released (or required) when the unrelaxed adsorbate components (i.e., before the geometry

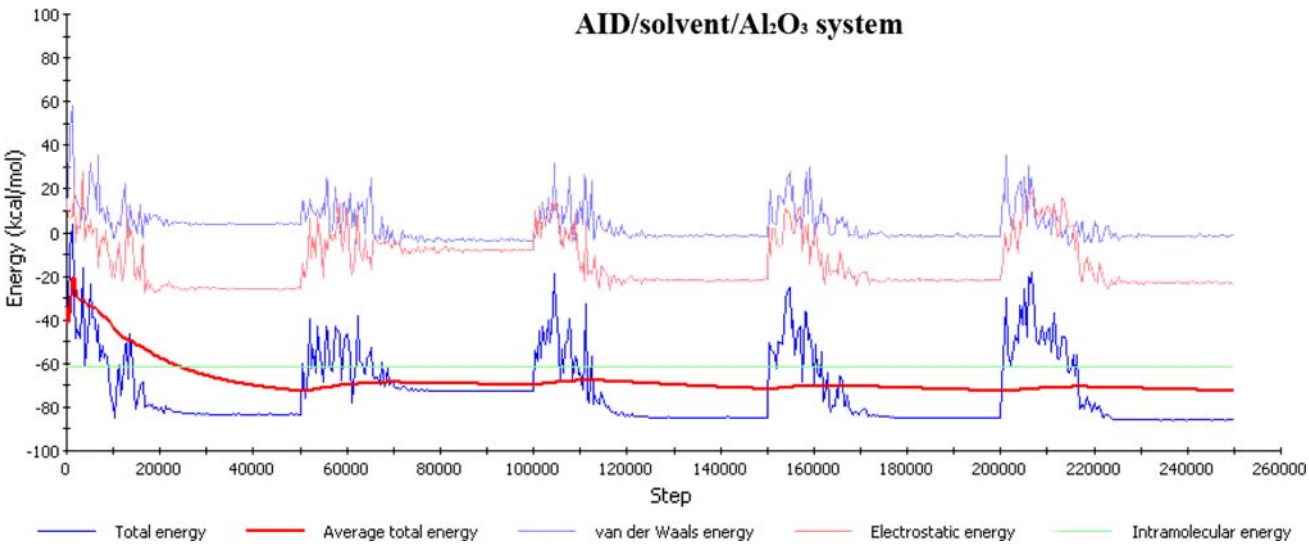

Fig. 5 Total energy distribution for AID/solvent/Al_2O_3 system

Table 4 Outputs and descriptors calculated by the Monte Carlo simulation for adsorption of AID, AIC or IM on Al (111) surface

Inhibitor	Total energy/ kcal mol^{-1}	Adsorption energy/ kcal mol^{-1}	Rigid adsorption energy/ kcal mol^{-1}	Deformation energy/ kcal mol^{-1}	dE_{ad}/dN_i / kcal mol^{-1}	Calculated hydrogen bond/Å
AID	−462.030	−49.4966	−32.922	−16.5745	−49.4966	1.8
AIC	−446.719	−38.325	−28.4688	−9.8562	−38.325	2.1
IM	−224.7354	−31.1832	−26.4985	−3.6846	−31.18324	2.8

optimization step) are adsorbed on the substrate. The deformation energy reports the energy released when the adsorbed adsorbate components are relaxed on the substrate surface. Table 4 also shows, (dE_{ads}/dN_i) which defines the energy of substrate–adsorbate configurations where one of the adsorbate components has been removed. As can be seen from Table 4, AID gives the maximum adsorption energy found during the simulation process (−49.49 kcal mol^{-1}). High values of adsorption energy confirm experimental results and explain why AID gives the highest inhibition efficiency. The close contacts between the imidazole derivatives and Al_2O_3 surface as well as the best adsorption configuration for the studied compounds are shown in Fig. 6.

For the purpose of determining the active sites of the inhibitor molecules, three influence factors: natural atomic charge, distribution of frontier molecular orbital, and Fukui indices are considered. According to classical chemical theory, all chemical interactions are by either electrostatic or orbital. Electrical charges in the molecule were obviously the driving force of electrostatic interactions. It has been proven that local electron densities or charges are important in many chemical reactions and physicochemical properties of compound [41]. The optimized geometries of the imidazole derivatives as well as the nature of their molecular orbitals, HOMO (highest occupied molecular orbital) and LUMO (lowest unoccupied molecular orbital) are involved in the properties of activity of imidazole derivatives and presented in Fig. 7.

The effectiveness of an inhibitor can be related with its electronic and spatial molecular structure. Also, there are certain quantum-chemical parameters that can be related to the interactions of metal-inhibitor, these are: the HOMO energy that is often associated with the capacity of a molecule to donate electrons, the energy gap ΔE (the lower values of energy gap, the better corrosion inhibition), and the dipole moment because low values will favor the accumulation of inhibitor molecules on the metallic surface [42]. A good correlation between the rate of corrosion and E_{HOMO}, as well as with energy gap ($\Delta E = E_{LUMO} - E_{HOMO}$) has been found in previous works [43, 44].

In Table 5, several quantum-chemical parameters related to the molecular electronic structure are presented. These theoretical parameters were calculated in liquid as well as in gas phase. The calculated parameters in gas phase as well as in the presence of a solvent do not exhibit important differences. The solvent in these calculations regarded as a continuous of uniform dielectric constant (ε) and the solute is placed in a cavity within it [45].

The HOMO energy can indicate the disposition of the molecule to donate electrons to an appropriated acceptor

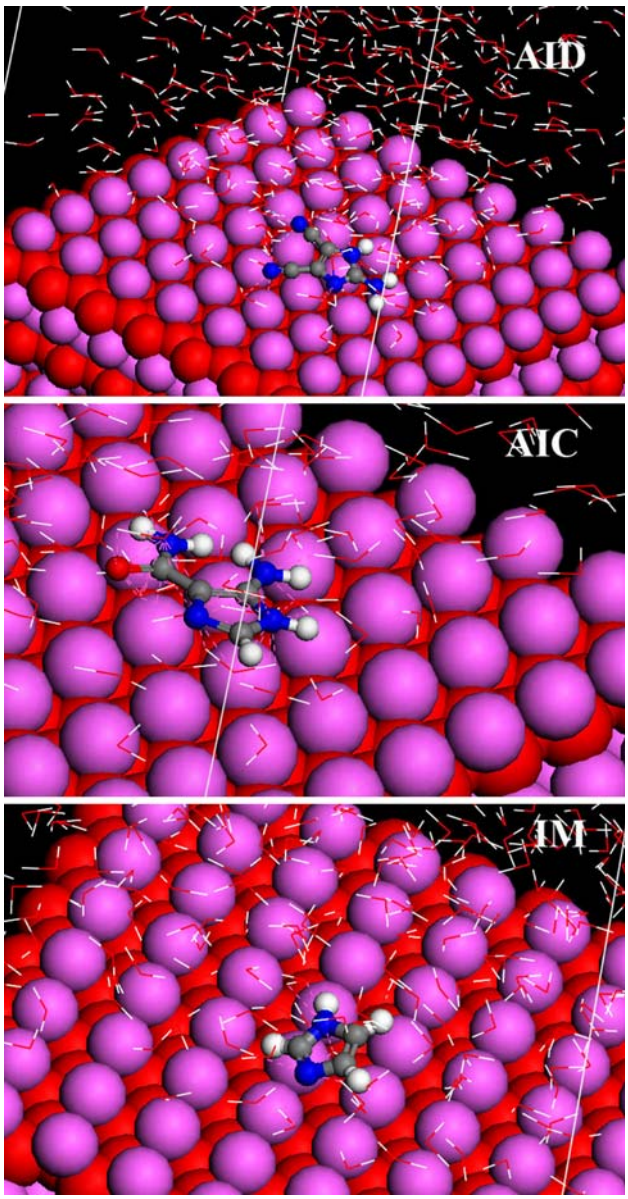

Fig. 6 Modes of adsorption of AID, AIC, and IM on Al_2O_3 surface (111)

with empty molecular orbitals (*p*-orbital in aluminum). Also, an increase in the values of E_{HOMO} can facilitate the adsorption, and therefore improved inhibition efficiency results [46]. The corrosion rate must decrease with increase in HOMO energy (less negative) [43]. Therefore an increase in the corrosion inhibition results (see Table 5).

Low values of the energy gap (ΔE) will provide good inhibition efficiencies, because the excitation energy to remove an electron from the last occupied orbital will be low [47]. The results show that the inhibitor AID has the lowest energy gap; this agrees with the experimental results that this molecule could have better performance as a corrosion inhibitor (see Table 5).

The HOMO location in the molecules is mostly distributed in the imidazole ring as well as amino groups indicating that the preferred sites for the electrophilic attack through metallic cations are located on the nitrogen atoms. It is probably that the parts of the molecules with high HOMO density were oriented toward the aluminum oxide surface and the adsorption of these ones could be sharing the lone pair electrons of nitrogen atoms and the π-electrons of the aromatic ring [48].

Table 6 shows Mulliken atomic charges calculated for the studied molecules. It is inferred that the more negative the atomic charges of the adsorbed center, the more easily the atom donates its electrons to the unoccupied orbital of the metal. It is clear from Table 6, that nitrogen and oxygen as well as some carbon atoms carrying negative charges centers which could offer electrons to the Al_2O_3 surface to form a coordinate bond.

The local reactivity has been analyzed by means of the Fukui Indices (FI) [49], since they indicate the reactive regions, in the form of the nucleophilic and electrophilic behavior of each atom in the molecule. The Fukui function $f(r)$ is defined as the first derivative of the electronic density $\rho(r)$ with respect to the number of electrons N at a constant external potential $v(r)$. Thus, using a scheme of finite differences, we had [50]:

$$f^{+}(r) = \rho_{N+1}(r) - \rho_N(r) \text{ (for nucleophilic attack)} \quad (15)$$

$$f^{-}(r) = \rho_N(r) - \rho_{N-1}(r) \text{ (for electrophilic attack)} \quad (16)$$

where ρ_{N+1}, ρ_N, and ρ_{N-1} are the electronic densities of anionic, neutral and cationic species, respectively. The N corresponds to the number of electrons in the molecule. $N + 1$ corresponds to an anion, with an electron added to the LUMO of the neutral molecule. $N - 1$ correspondingly is the cation with an electron removed from the HOMO of the neutral. All calculations are done at the ground-state geometry. These functions can be condensed to the nuclei by using an atomic charge partitioning scheme, such as Mulliken population analysis in Eqs. 15 and 16).

An easy graphical display technique can also be used based on the Fukui functions. Instead of calculating the molecular orbitals for the neutral, cation, and anion, we can just add or subtract electrons from the molecular orbitals of the neutral molecule. This procedure is not as good as described above, but it does give a quick graphical display of the susceptibility of different kinds of attack. So rather than being a definitive calculation of a molecular property, freezing the molecular orbitals to those for the neutral molecule gives a useful graphical technique that can be rapidly applied.

The FI calculations were performed with Dmol^3 using a Mulliken population analysis [51] or a numerical integration procedure such as a Hirshfeld analysis [52]. The $f^{+}(r)$ measures the density of changes when the molecule gains

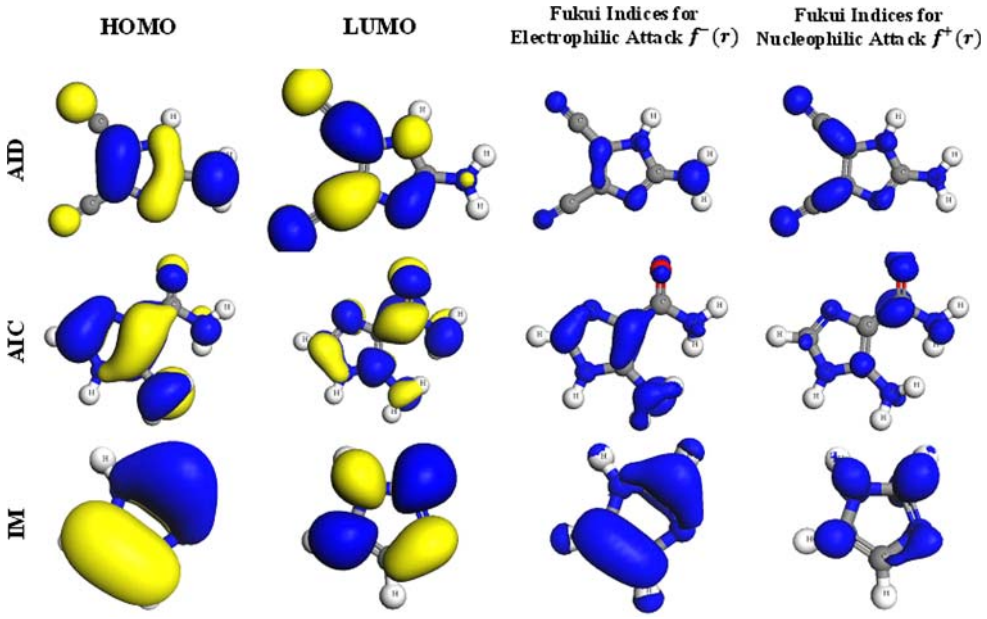

Fig. 7 Molecular orbital plots as well as active sites for electrophilic and nucleophilic attack on AID, AIC, and IM

Table 5 HOMO and LUMO energies, HOMO–LUMO gap (ΔE) and dipole moment μ for AIC, AID and IM obtained in the gas phase and in the presence of water, respectively

Inhibitor	E_{HOMO}/ eV	E_{LUMO}/ eV	$\Delta = E_{LUMO} - E_{HOMO}$/ eV	μ/(D)
AID	−8.535	0.3035	8.8385	8.115
	−8.632	0.3136	8.9456	8.123
AIC	−9.0257	0.4321	9.4578	8.277
	−9.1254	0.4542	9.5796	8.3214
IM	−9.467	0.6962	10.1632	9.125
	−9.8745	0.7213	10.5958	9.2150

electrons and it corresponds to reactivity with respect to nucleophilic attack. On the other hand, $f^-(r)$ corresponds to reactivity with respect to electrophilic attack or when the molecule losses electrons.

The FI values are presented in Table 6. AID has propitious zones for nucleophilic attack located on N2, C3, N7, N9 while AIC has only on C1, C4, C6, O7, N9. Imidazole ring has only nucleophilic centers on (C6 and O7). Data in Table 6 shows that AID has more susceptible sites for adsorption on the aluminum surface, which again reflects its highest inhibition performance. The HOMO location on each system agrees with the atoms that exhibit greatest values of indices of Fukui (Fig. 7), both indicate the zones by which the molecule would be adsorbed on the Al_2O_3 surface (see Fig. 7).

3.5 Adsorption isotherm

A direct relationship between inhibition efficiency and the degree of surface coverage (θ) can be assumed for different concentrations of the inhibitor. Data obtained from weight loss measurements were tested graphically for fitting various adsorption isotherms including Langmuir, Frumkin, and Temkin. By far for these compounds the best fit was obtained with the Langmuir adsorption isotherm (Fig. 8). According to this isotherm θ is related to inhibitor concentration by the following equations [53].

$$\frac{C_{inh}}{\theta} = \frac{1}{b} + C_{inh} \tag{17}$$

$$b = \frac{1}{55.5}\exp\left(-\frac{\Delta G_{ads}}{RT}\right) \tag{18}$$

C_{inh} is the inhibitor concentration, θ is the fraction of the surface covered, b is the adsorption coefficient and ΔG_{ads} is the standard free energy of adsorption. The value of 55.5 being the concentration of water in solution expressed in mole.

The degree of surface coverage (θ) for different concentrations of imidazoles in the acid has been evaluated from weight loss measurements values. The values of θ have been inserted in Table 1. The degree of surface coverage was found to increase with increasing the concentration of the imidazole derivatives. The obtained plots of the inhibitors are linear with correlation coefficient higher than 0.99. The intercept permits the calculation of the equilibrium constant b which is 13440.86, 9335.84, and 4878.04 M^{-1} for AID, AIC, and IM, respectively. The values of b, which indicate the binding power of the imidazole derivatives to the aluminum surface, were used to calculate the adsorption energy, ΔG_{ads}. The recorded values of ΔG_{ads} were −34, −32.6, and −30.9 kJ mol^{-1} for AID, AIC, and IM, respectively. The large values of ΔG^0_{ads} and its negative sign are usually characteristic of strong interaction and a highly efficient adsorption [54]. The high

Table 6 Calculated Mulliken atomic charges and Fukui functions for the three selected imidazoles

	Atom	q_N	q_{N+1}	q_{N-1}	f_k^+	f_k^-	f_k^o
AID	C(1)	0.557	0.600	0.412	0.043	0.145	0.044
	N(2)	−0.382	−0.311	−0.477	0.071	0.095	0.083
	C(3)	0.155	0.235	0.064	0.080	0.091	0.065
	C(4)	0.230	0.296	0.142	0.066	0.088	0.077
	N(5)	−0.580	−0.533	−0.646	0.047	0.066	0.041
	C(6)	0.187	0.256	0.155	0.069	0.032	0.050
	N(7)	−0.319	−0.138	−0.466	0.181	0.147	0.164
	C(8)	0.163	0.242	0.115	0.079	0.048	0.064
	N(9)	−0.322	−0.134	−0.489	0.188	0.167	0.178
	N(10)	−0.789	-0.751	−0.904	0.038	0.115	0.077
	H(11)	0.367	0.422	0.294	0.055	0.073	0.054
	H(12)	0.374	0.414	0.285	0.040	0.089	0.049
	H(13)	0.358	0.402	0.295	0.044	0.063	0.054
AIC	C(1)	0.024	0.073	−0.122	0.049	0.146	0.077
	N(2)	−0.288	−0.230	−0.383	0.058	0.095	0.067
	C(3)	0.111	0.109	−0.006	−0.002	0.117	0.042
	C(4)	0.390	0.487	0.225	0.097	0.165	0.081
	N(5)	−0.498	−0.477	−0.537	0.021	0.039	0.020
	C(6)	0.404	0.561	0.367	0.157	0.037	0.097
	O(7)	−0.426	−0.253	−0.546	0.173	0.120	0.147
	N(8)	−0.809	−0.782	−0.840	0.027	0.031	0.014
	N(9)	−0.825	−0.777	−0.946	0.048	0.121	0.084
	H(10)	0.160	0.240	0.059	0.080	0.101	0.090
	H(11)	0.344	0.405	0.281	0.061	0.063	0.062
	H(12)	0.351	0.413	0.325	0.062	0.026	0.044
	H(13)	0.352	0.422	0.295	0.070	0.057	0.063
	H(14)	0.342	0.407	0.269	0.065	0.073	0.069
	H(15)	0.368	0.401	0.319	0.033	0.049	0.041
IM	C(1)	0.016	0.203	−0.122	0.187	0.138	0.162
	N(2)	−0.279	−0.180	−0.370	0.099	0.091	0.095
	C(3)	−0.104	−0.055	−0.211	0.049	0.107	0.078
	C(4)	−0.090	0.053	−0.246	0.143	0.156	0.150
	N(5)	−0.406	−0.353	−0.427	0.053	0.021	0.037
	H(6)	0.145	0.277	0.016	0.132	0.129	0.131
	H(7)	0.137	0.255	0.001	0.118	0.136	0.127
	H(8)	0.146	0.273	0.008	0.127	0.138	0.132
	H(9)	0.336	0.430	0.252	0.094	0.084	0.089

values of ΔG^0_{ads} show that, in the presence of 1.0 M HCl chemisorptions of imidazole derivatives may occur.

The free adsorption energies calculated from Langmuir adsorption isotherm are in line with adsorption energies calculated from Monte Carlo simulation method. The difference in the values of adsorption energy calculated from Monte Carlo simulations and Langmuir adsorption isotherm could be explained by adsorption of surface aggregates. Although it appears that the adsorbate structure on corroding metals has not been investigated, it is quite possible that such structures are formed in the initial stage of adsorption [55].

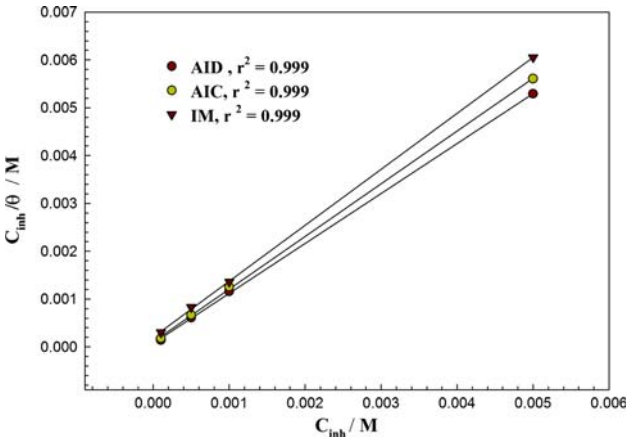

Fig. 8 Langmuir's adsorption plots for Al in 1.0 M HCl solutions containing various concentrations of AID, AIC or IM at 25 ± 1 °C

3.6 Mechanism of inhibition

It is well-known that terminal oxygen atoms at metal oxide surfaces react with water, forming hydroxylated sites, or hydroxide layers at the surface (M–OH), that impart a pH-dependent surface charge. The polar hydroxyl ($-OH^-$) groups may cause the surface to attract and physically adsorb a single or several additional layers of polar water molecules. An oxide or hydroxide surface (Al–OH) becomes charged by reacting with H^+ or OH^- ions due to surface amphoteric reactions as presented in equations:

$$Al - OH + H^+ \rightleftarrows Al - OH^{2+} \quad (19)$$

$$Al - OH + OH^- \rightleftarrows Al - O^- + H_2O \quad (20)$$

In 1.0 M HCl, where pH is low, hydroxide surface adsorbs protons to produce positively charged surfaces $\left(Al - OH_2^+\right)$.

The number of these sites and the surface charge of the oxide are determined by the pH of the solution. Surface charge influences adsorption of ions from solution and other interfacial phenomena [56]. The pH of the potential of zero charge (PZC) for aluminum oxides/hydroxides is between 6 and 9, and in acidic solution, the accumulation of $Al - OH_2^+$ species accounts for the surface charge [57, 58]. In acidic solution, therefore the positively charged surface sites electrostatically attract any anions present in solution, and repel cations.

It is a general assumption that the adsorption of the organic inhibitors at the metal solution interface is the first step in the mechanism of the inhibitor action. Organic molecules may adsorbed on the metal surface in four types: (a) electrostatic interaction between a negatively charged surface, which is provided with specifically adsorbed anions (Cl^-) on aluminum and the positive charge of the

inhibitor, (b) interaction of unshared electron pairs in the molecule with the metal, (c) interaction of π-electron with metal, and (d) a combination of the (a–c) types. Efficient adsorption is the result of either π-electron of the imidazole system or the electronegative N (heteroatom) atoms [59].

The adsorption of imidzole compounds can be described by two main types of interaction: physical adsorption and chemisorption. In general, the proceeding of physical adsorption requires the presence of both electrically charged surface of the metal and charged species in the bulk of the solution. Chemisorption process involves charge sharing or charge transfer from the inhibitor molecules to the metal surface to form a coordinate type of a bond. This is possible in case the of positive as well as negative charge of the surface.

However, the inhibitors under investigation, namely imidazole derivatives are organic bases which protonize in an acid medium. Thus, the inhibitor molecules become a cation, existing in equilibrium with the corresponding molecular form. The electrostatic adsorption of these cations could be explained on the basis that Cl^- ions first adsorbed at the electrode/solution interface at the corrosion potential through electrostatic attraction force due to the excess positive charge at the interface. This process changes the charge of the solution side of the interface from positive to negative, and thus facilitating physical adsorption of the inhibitors' cations. Thus, cations of these compounds are able to electrostatically adsorb on the electrode surface covered with primary adsorbed Cl^- ions, see Fig. 9a. The adsorption of imidazole derivatives on the

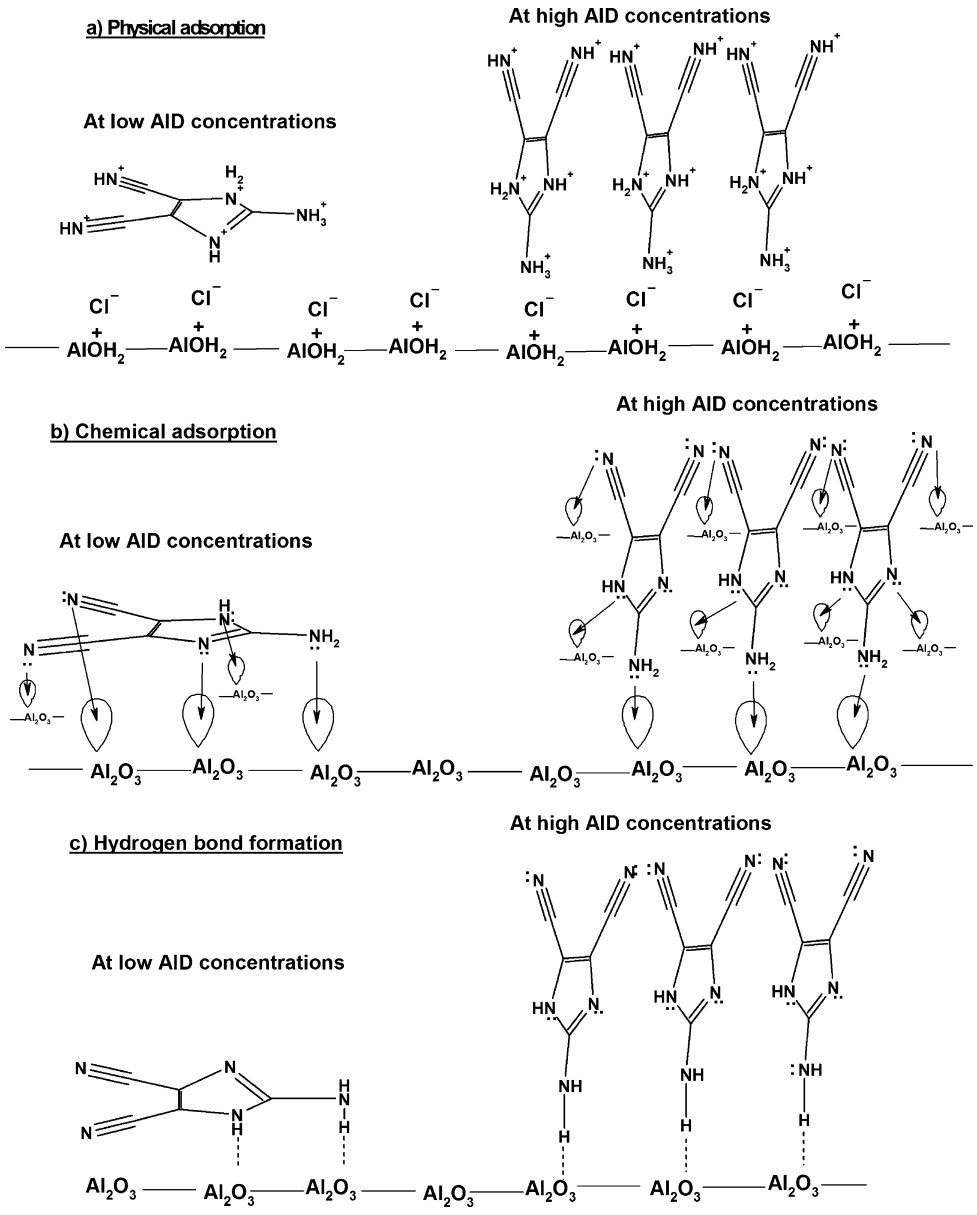

Fig. 9 Different modes of adsorption of AID, as a representative example, on Al oxide surface at E_{corr}

electrode surface makes a barrier for mass and charge transfers. This situation leads to the protection of the electrode surface from the acid corrosion.

In addition to the physical (electrostatic) adsorption, there should be a chemical adsorption, see Fig. 9b, due to the coordinate type of bonds that may be formed, between the lone electron pairs of the unprotonated N-atoms and the empty *p*-orbital of Al atoms which enhance the attraction between the imidazole derivatives and the electrode surface. The chemical adsorption is probably the most important type of interaction between the Al_2O_3 surface and the imidazole derivatives. Here, the adsorbed species are in contact with the Al_2O_3 surface. In this process, a coordinated bond that involves the electron transference from inhibitor system toward the metallic surface is formed.

The electron transference is facilitated when the inhibitor molecule has a lone pair of electrons without sharing in the donating atom of the functional group, and the availability of π-electrons due to the presence of double bonds or aromatic rings in its structure. Moreover, there is a great possibility that adsorption may also take place via hydrogen bond formation between the N–H linkage in imidazole derivatives and the oxygen atoms of the oxidized surface species, Fig. 9c. This type of adsorption should be more prevalent for protonated N-atoms, because the positive charge on the N-atom is conductive to the formation of hydrogen bonds. Unprotonated N-atoms may adsorb by direct chemisorption, as mentioned previously, or by hydrogen bonding to a surface oxidized species. The extent of adsorption by the respective modes depends on the nature of the metal surface. Adsorption by direct chemisorption, for unprotonated N-atom, is more probable on an exposed metal atom. In addition, the unprotonated N-atom can also interact with oxidized metal by hydrogen bonding. Effective inhibition is predominantly provided by the direct coordination of unprotonated N-atom to metal atoms. As the metal surface is covered by an adherent oxide protective layer, the direct coordination of nitrogen to an exposed metal atom is a remote event. Protonated and unprotonated N-atoms are adsorbed onto the metal through hydrogen bond formation. The criteria for inhibitor selection can also be inferred from above considerations. A good inhibitor must have strong affinity for the bare metal atoms. The requirement is different in case of aluminum; a compact passive oxide film is always present on the electrode surface, where hydrogen bond formation accounts for most of the inhibition action. An effective inhibitor is one that forms hydrogen bonds easily with the oxidized surface.

Elucidating the orientation of organic molecules on the electrode surface different factors need to be considered [60]. In the case of the studied imidazole derivatives, the atoms and groups that may interact with the electrode surface are the N atoms either in the diazole ring and its substituent in addition, the double and triple bonds present in the studied molecules. The delocalization of π-electrons in the imidazole ring may weakly interact with the aluminum oxide surface when molecules are oriented horizontally [60], but they may also interact with other imidazole molecules forming parallel double coin-stacks, with AID molecules oriented vertically (Fig. 9). The interactions of nitrogen-containing heterocyclic molecules with metal surfaces through N-atoms have long been postulated for imidazole derivatives, pyridine, BTA, etc. The proposed orientations ranged from horizontal for oleic imidazoline [61], to vertical for pyridine [62].

Orientation of the studied inhibitors on aluminum oxide surface has been presented in Fig. 9. It is clear that the orientation of the imidazole derivatives depends on their concentrations. In the early stages of adsorption (at low surface coverage), i.e., low concentrations, the orientation of the studied molecules is parallel to the aluminum oxide surface. As the concentrations of the inhibitor molecules increased more surface coverage occurs and the inhibitor molecules are oriented vertically as in Fig. 9. By increasing the inhibitors concentrations the formed barrier becomes more compact and protective with adsorption of more AID molecules on the surface. In this way, the inhibition efficiency of imidazole derivatives increases with increase in concentration.

4 Conclusion

Chemical and electrochemical measurements incorporated with molecular dynamics simulations were used to study the corrosion inhibition characteristics of some imidazole derivatives on aluminum in aerated stagnant 1.0 M HCl solutions. The principle conclusions are as follow:

- Addition of imidazole derivatives effectively reduces the corrosion of aluminum in 1.0 M HCl.
- Inhibition efficiency of these compounds increases with increase in their concentrations due to the formation of a surface film on the aluminum surface.
- Monte Carlo simulations technique incorporating molecular mechanics and molecular dynamics can be used to simulate the adsorption of imidazole derivatives on aluminum (111) surface in 1.0 M HCl.
- Physisorption, followed by chemisorption is proposed as the mechanism for the inhibition process which is enhanced via formation of hydrogen bonding.

References

1. Li X, Nie X, Wang L, Northwood DO (2005) Surf Sci Coat Technol 200:1994
2. Sherif EM, Park SM (2006) Electrochim Acta 51:1313

3. Talbot D, Talbot J (1998) Corrosion science and technology. CRC Press LLC, Florida
4. Ovari F, Tomcsanyi L, Turmezey T (1998) Electrochim Acta 33:323
5. Tomcsanyi L, Varga K, Bartik I, Horanyi G, Maleczki E (1989) Electrochim Acta 34:855
6. Stevanovic RM, Despic AR, Drazic DM (1988) Electrochim Acta 33:397
7. Ashassi-Sorkhabi H, Shabani B, Aligholipour B, Seifzadeh D (2006) Appl Surf Sci 252:4039
8. Khaled KF, Qahtani M (2009) Mater Chem Phys 113:150
9. Abdel Kader JM, Shams El Din AM (1970) Corros Sci 10:551
10. Sampat SS, Vora JC (1974) Corros Sci 14:591
11. Shalaby LA, El Sobki KM, Abdel Azim AA (1976) Corros Sci 16:637
12. El Mahdy GA, Mahmoud SS (1995) Corros Sci 51:436
13. Khaled KF (2003) Electrochim Acta 48:2493
14. Chetouani A, Hammouti B, Benhadda T, Daoudi M (2005) Appl Surf Sci 249:375
15. Lebrini M, Lagrenee M, Vezin H, Gengembre L, Bentiss F (2005) Corros Sci 47:485
16. Solmaz R, Kardas G, Yazıcı B, Erbil M (2005) Prot Met 41:581
17. Ozcan M, Karadag F, Dehri I (2008) Colloids Surf A 316:55
18. Bereket G, Ogretir C, Ozsahim C (2004) J Mol Struct (THEOCHEM) 663:173
19. Li Y, Zhao P, Liang Q, Hou B (2005) Appl Surf Sci 252:1245
20. Ogretir C, Mihci B, Bereket G (1999) J Mol Struct (THEOCHEM) 488:223
21. Barriga J, Coto B, Fernandez B (2007) Tribol Int 40:960
22. Sun H, Ren P, Fried JR (1998) Comput Theor Polym Sci 8:229
23. Ebenso EE, Okafor PC, Ekpe UJ (2002) Bull Electrochem 18:553
24. Nguyen TH, Foley RT (1982) J Electrochem Soc 129:32
25. Al-Mayouf AM (1996) Corros Prev Control 6:70
26. Ford FP, Burstein GT, Hoar TP (1980) J Electrochem Soc 127:1325
27. Oguzie EE, Okolue BN, Ebenso EE, Onuoha GN, Onuchukwu AI (2004) Mater Chem Phys 87:401
28. Vracar LM, Drazic DM (2002) Corros Sci 44:1669
29. McCafferty E (2005) Corros Sci 47:3202
30. Branzoi V, Golgovici F, Branzoi F (2002) Mater Chem Phys 78:122
31. Brett CMA (1989) Port Electrochem Acta 7:123
32. Lenderink HJW, Linden MVD, Wit JHWDE (1993) Electrochim Acta 38:1989
33. Brett CMA (1990) J Appl Electrochem 20:1000
34. Frers SE, Stefenel MM, Mayer CM, Chierchie T (1990) J Appl Electrochem 20:996
35. Abdel-Gaber AM, Khamis E, Abo-ElDahab H, Sh Adeel (2008) Mater Chem Phys 109:297
36. McCafferty E, Hackerman N (1972) J Electrochem Soc 119:146
37. Bataillon C, Brunet S (1994) Electrochim Acta 39:455
38. Kissi M, Bouklah M, Hammouti B, Benkaddour M (2006) Appl Surf Sci 252:4190
39. Bentiss F, Lagrenee H, Traisnel M, Hornez JC (1999) Corros Sci 41:789
40. Oskes G, Vest JM (1969) Br Corros J 4:6617
41. Karelson M, Lobanov VS (1996) Chem Rev 96:1027
42. Lukovits I, Pálfi K, Bakó I, Kálmán E (1997) Corrosion 53:915
43. Sastri VS, Perumareddi JR (1997) Corros Sci 53:617
44. Lukovits I, Kálmán E, Zucchi F (2001) Corrosion 57:3
45. Foresman JB, Frisch Æ (1996) Exploring chemistry with electronic structure methods, 2nd edn. Gaussian Inc., Pittsburgh, PA
46. Khalil N (2003) Electrochim Acta 48:2635
47. Bentis F, Traisnel M, Vezin H, Hildebrand HF, Lagrenée M (2004) Corros Sci 46:2781
48. Martínez S, Štagljar I (2003) J Mol Struct (THEOCHEM) 640:167
49. Yang W, Mortier WJ (1986) J Am Chem Soc 108:5708
50. Lee C, Yang W, Parr RG (1988) J Mol Struct (THEOCHEM) 163:305
51. Mulliken RS (1955) J Chem Phys 23:1833
52. Hirshfeld FL (1977) Theor Chim Acta B44:129
53. Khaled KF (2008) Electrochim Acta 53:3484
54. Abdallah M (2002) Corros Sci 44:717
55. Knag M, Sjöblom J, Øye G, Gulbrandsen E (2005) Colloids Surf A 250:269
56. Brown GE (1999) Chem Rev 99:647
57. Hohl H, Stumm M (1976) J Colloid Int Sci 55:281
58. Wood R, Formasiero D, Ralston J (1990) Colloid Surf 51:389
59. Emregul KC, Atakol O (2004) Mater Chem Phys 83:373
60. Scendo M, Hepel M (2008) J Elecroanal Chem 613:35
61. Edwards A, Osborn C, Webster S, Kleinerman D, Joseph M, Ostovar P, Doyle M (1994) Corros Sci 36:315
62. Conway BE, Barradas RG (1961) Electrochim Acta 5:319